Auton Robot (2011) 31:225–234
DOI 10.1007/s10514-011-9242-3

Passive torque regulation in an underactuated flapping wing robotic insect

P.S. Sreetharan · R.J. Wood

Received: 1 November 2010 / Accepted: 28 June 2011 / Published online: 20 July 2011

Abstract Recent developments in millimeter-scale fabrication processes have led to rapid progress towards creating airborne flapping wing robots based on Dipteran (two winged) insects. Previous work to regulate forces and torques generated by flapping wings has focused on controlling wing trajectory. An alternative approach uses underactuated mechanisms with tuned dynamics to passively regulate these forces and torques. The resulting 'mechanically intelligent' devices execute wing trajectory corrections to realize desired body forces and torques without the intervention of an active controller.

This article describes an insect-scale flapping wing mechanism consisting of a single piezoelectric actuator, an underactuated transmission, and passively rotating wings. Wing stroke velocities are passively modulated to eliminate net airframe roll torque. A theoretical model predicts lift generating wing trajectories and quantifies the passive reduction in roll torque. An experimental structure provides an at-scale demonstration of passive torque regulation.

Keywords Linkages · Kinematics · Dynamics · Bio-inspired robotics · Micro air vehicles · Passive mechanisms

1 Introduction

Advances in millimeter scale fabrication processes have enabled rapid progress towards the development of flapping wing micro air vehicles (FWMAVs) with system mass on the order of 100 mg (Wood 2008). However, flight stability and control mechanisms for these mass and power limited systems remain active areas of research.

Investigation into the aerodynamics of biological insect flight has produced approximate aerodynamic models allowing computationally inexpensive prediction of aerodynamic forces and torques from wing trajectories (Dickinson et al. 1999; Dickson et al. 2006). Accordingly, research into transmission and control mechanisms of flapping wing robotic insects has focused on control of wing trajectory. For example, the Berkeley Micromechanical Flying Insect (MFI) is a FWMAV platform with the ability to execute a range of predetermined wing trajectories using a fully actuated wing drive mechanism, neglecting elastic deformation of the transmission and wings (Fearing et al. 2001). In one notable exception, the Harvard Microrobotic Fly (HMF) has proven capable of realizing qualitatively biomimetic wing trajectories using passive compliance to allow variation of wing angles of attack (Wood 2008). The associated reduction in complexity has allowed this aeromechanical platform to achieve a lift to weight ratio greater than one.

However, the benefits of underactuation and passive compliance can extend beyond simple reduction of mechanical complexity, in particular for devices in which the distribution of forces and torques is more important than device configuration. A ubiquitous example is the automobile differential, an underactuated mechanism commonly used to distribute engine power to two wheels. The differential incorporates an additional degree of freedom q_2 to balance the torque delivered to each wheel (see Fig. 1). The differential fundamentally operates on wheel torques instead of rotations; aided by passive mechanisms, the wheels can rotate along complex relative trajectories, maintaining traction on the ground without closed loop active control.

P.S. Sreetharan (✉) · R.J. Wood
Harvard Microrobotics Laboratory, 60 Oxford St. #407, Cambridge, MA 02138, USA
e-mail: pratheev@post.harvard.edu

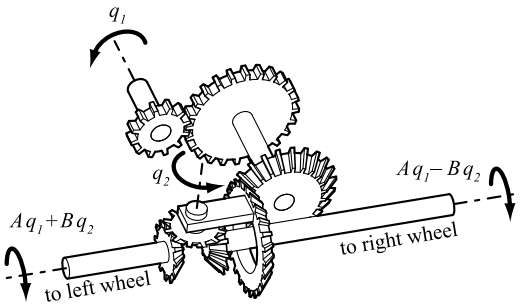

Fig. 1 A car differential balances output torques using an underactuated mechanism. Degree of freedom q_1 receives engine torque while q_2 is unactuated

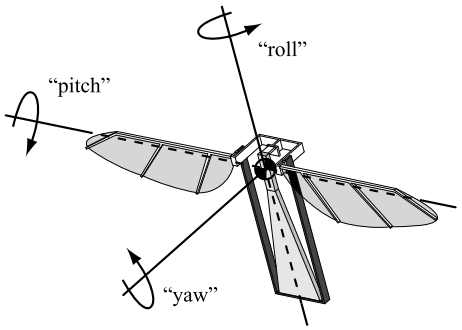

Fig. 2 Definition of roll, pitch, and yaw in the body frame

Previous work has introduced the concept of Passive Aeromechanical Regulation of Imbalanced Torques (PARITy) in the context of insect-scale FWMAV design (Sreetharan and Wood 2010). Embodying the PARITy concept, the 'Drag PARITy' is an underactuated two degree of freedom FWMAV transmission that, analogous to an automobile differential, passively distributes power from a single actuator to balance torques delivered to two wings. The Drag PARITy was shown to passively balance drag induced roll torque within a planar two degree of freedom system, but in this study wings were rigidly attached to the transmission output and had fixed 90° angles of attack. Since the wings remained perpendicular to the relative wind, they produced drag but no lift. Producing lift from flapping wings requires varying wing rotation (illustrated as ψ^R in Fig. 3c) during operation.

This paper describes an evolution of the FWMAV design from Sreetharan and Wood (2010); a compliant 'wing hinge' (Fig. 3c) has been incorporated into the base of the wing, similar to the approach taken by Wood (2008). This change is a mechanistically simple passive technique for allowing wing rotation to vary over the wingstroke, resulting in the capability to produce aerodynamic lift. This mechanical simplicity, however, does not translate into dynamic simplicity. The difficulty of describing the behavior of the nonplanar, four degree of freedom system presented in this paper significantly exceeds that of the planar two degree of freedom system previously tested.

The underactuated flapping wing system is shown to execute stable, qualitatively biomimetic, lift-generating wing trajectories, indicating that the Drag PARITy is a viable transmission design for insect-scale FWMAVs. A theoretical model of the system is developed to investigate torque balancing characteristics in simulation. A control ('Uncut') trial with a nominally symmetric system demonstrates passive balancing of roll torques imparted from each wing, compensating for fabrication variation. In '1-Cut' and '2-Cut' trials, the system is simulated with successive removal of planform area from one wing (to provide an asymmetric disturbance) and is shown to continue successfully balancing roll torques, compensating for large inertial and aerodynamic wing asymmetries. By passively diverting more power to an underperforming wing, the design is also shown to indirectly compensate for imbalanced lift generation. Finally, an at-scale test device is constructed and observed to execute wing trajectories supporting theoretical predictions. Prior to describing the experiment, however, the PARITy methodology for FWMAV control which motivates this investigation will first be outlined.

2 The PARITy methodology

Though it would allow for a highly capable FWMAV, fully-actuated high-bandwidth control of wing trajectories has not been achieved on a 100 mg platform. Millimeter-scale fabrication techniques have not yet demonstrated the requisite complexity within mass constraints. Furthermore, power and mass constraints are likely to limit the bandwidth of electronic sensing and control systems on these lightweight platforms.

Acknowledging these limitations, research has been conducted into 'time-averaged' wing control, seeking to control average forces and torques by applying kinematic wing trajectory corrections on timescales longer than a wing flapping period (Deng et al. 2006). Assuming that active control will not be attempted at short (sub-wingbeat) timescales, the question of the ideal short timescale behavior of a wing flapping mechanism is raised. Conventional kinematic control approaches tacitly assume that rigid specification of wing trajectory is a preferred short timescale behavior.

However, the specific wing trajectory executed is not fundamentally important to an FWMAV. Rather, an active flight control system will treat wing trajectory as merely a tool to generate desired reaction forces and torques on the airframe. Ideally, the wings should execute whatever trajectories are necessary to realize these desired forces and torques.[1] A drivetrain that passively regulates these forces

[1]The specific trajectory may be important for efficiency concerns, but is irrelevant for the purposes of stabilizing and controlling the airframe.

and torques at a short timescale may simplify a longer timescale flight controller.

This alternative short term behavior is conjectured to produce systems that reject short timescale disturbances passively, alleviating requirements on active control systems. It is also expected to compensate for a subset of fabrication asymmetries, passively realizing the necessary adjustments to wing trajectory. This feature is an attractive one, since fabrication variation is a major concern for devices manufactured at the millimeter scale.

Under the PARITy methodology, long timescale control is achieved not by altering the wing trajectories directly, but by modulating the dynamics of the short timescale passive system. In the context of PARITy based FWMAV designs, control inputs would perturb the setpoint of short timescale system dynamics. For example, the 'Drag PARITy' drivetrain analyzed in this paper passively balances body roll torques imparted by each wing. However, actuation of an active control input could bias system dynamics such that the magnitude ratio of roll torques imparted by the wings is passively regulated to a value other than one. This local passive regulation may enable direct active force and torque control at long timescales, simplifying the control problem for mass-limited flapping wing aeromechanical platforms.

Such active control mechanisms are the subject of future work and will not be discussed in depth in this paper, but their brief mention serves to motivate the detailed analysis of simpler PARITy drivetrains without control capability. The following sections analyze a specific FWMAV system introducing passively rotating wings to an actuated Drag PARITy transmission.

3 Components of a roll torque balancing FWMAV

3.1 Airframe

The airframe is a rigid mechanical structure, constructed of a lightweight carbon fiber reinforced polymer (CFRP). It serves as a mechanical ground, rigidly connecting the base of the actuator to ground points on the transmission mechanism. In future devices, the airframe will incorporate the other elements, such as power, sensing and active control, necessary for a fully autonomous robot.

3.2 Actuator

Piezoelectric actuation has been chosen due to its high bandwidth and high power density (Wood et al. 2005). The actuator is a bimorph PZT cantilever, with a peak-to-peak actuation stroke of approximately 500 μm. The base of the cantilever is grounded to the airframe, while the output is affixed to the transmission input (Fig. 3).

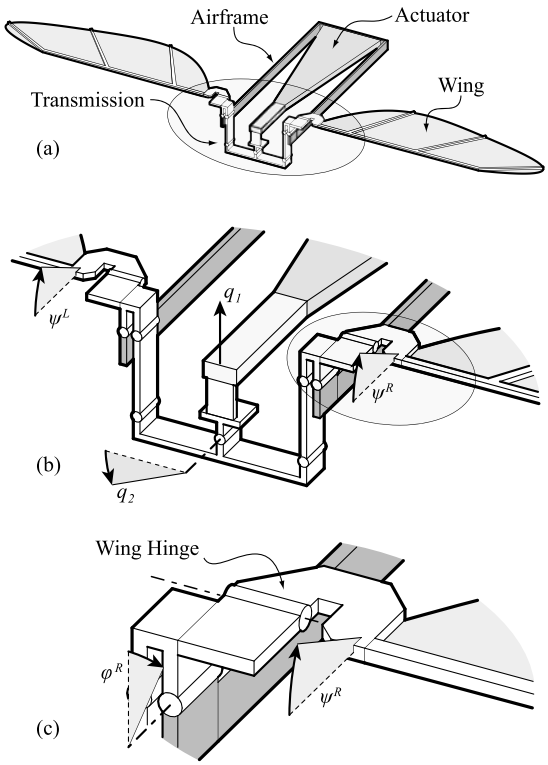

Fig. 3 (**a**) Diagram of the FWMAV design. (**b**) The four degrees of freedom q_1, q_2, ψ^L, and ψ^R with respect to airframe ground. (**c**) A view of the shoulder clarifying rotation angle ψ^R. Right wing stroke angle ϕ^R can be determined from q_1 and q_2, as can ϕ^L of the left wing (not shown)

3.3 Wings

Wings consist of a 1.5 μm polyester membrane supported by carbon fiber venation, shown in Fig. 5. Fabricated wings have masses under 1 mg and are effectively rigid plates, exhibiting limited deformation while flapping. In an approach pioneered by Wood (2008), each wing is attached to a transmission output in series with a polymer flexure 'wing hinge' that allows the rigid wing to passively rotate around its longitudinal axis (see Fig. 3c). Compliance of the wing hinge allows the angle of attack of each wing to vary passively while flapping.

3.4 Transmission

The Drag PARITy transmission is a millimeter scale planar linkage constructed using Smart Composite Microstructure (SCM) fabrication techniques (Wood et al. 2008). Unidirectional CFRP beams form rigid links, while revolute joints are realized by polymer flexure interconnects (Fig. 8). A primary function of the transmission is to map the 500 μm actuation stroke to the approximately 80°–120° peak-to-peak wingstroke. In addition to transmitting power to the wings,

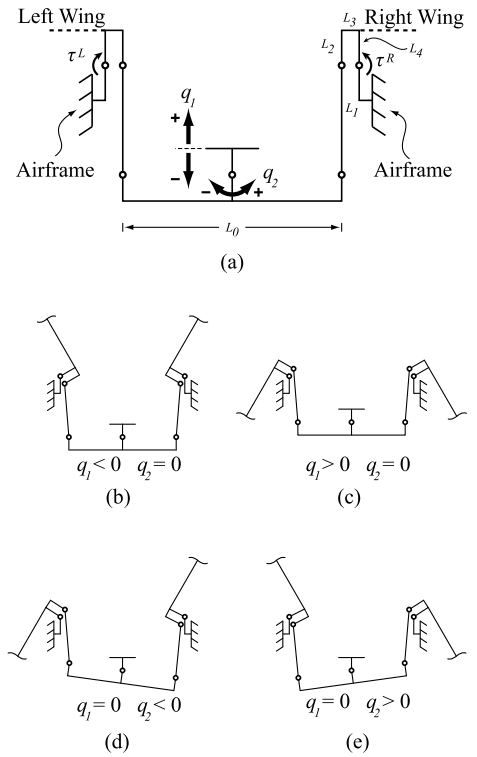

Fig. 4 (**a**) Planar kinematics of the two degree of freedom drag PARITy transmission. Holding $q_2 = 0$ and allowing q_1 to oscillate between (**b**) negative and (**c**) positive values produces a symmetric flapping motion. Holding $q_1 = 0$ and allowing q_2 to take (**d**) negative and (**e**) positive values produces a differential flapping motion, coupling the upstroke of one wing with the downstroke of the other

the Drag PARITy transmission incorporates a simple underactuated mechanism that passively modulates wing stroke velocities in response to imbalanced roll torques.

4 The Drag PARITy transmission

The Drag PARITy transmission has a single actuated input q_1 and dual outputs driving the stroke angles of each wing. The right wing stroke angle ϕ^R is illustrated in Fig. 3c, while the left wing stroke angle ϕ^L (not shown) is the analogous angle on the opposing wing. The transmission mechanism has two degrees of freedom; referring to Fig. 3b, q_1 is actuated and allows power to be injected into the system, while q_2 is passively determined.

The two degrees of freedom of the Drag PARITy transmission are illustrated in Fig. 4. The actuator output drives the transmission input q_1 in an oscillatory trajectory, while q_2 describes the rotation of the 'balance beam' link L_0. Figures 4b and 4c demonstrate the symmetric wingstrokes achieved by fixing $q_2 = 0$. Rotation of the balance beam through an angle q_2 couples the upstroke of one wing to the downstroke of the other, a feature central to the passive torque balancing properties of the Drag PARITy transmission. An invertible kinematic mapping relates q_1 and q_2 to the wing stroke angles ϕ^L and ϕ^R; the latter pair of coordinates are used in the theoretical model.

The passive torque balancing mechanism can be conceptually understood by considering the complete FWMAV system in operation. When the actuator is driven, the left and right wings execute a periodic flapping motion, exerting torques τ^L and τ^R, respectively, on the transmission outputs (see Fig. 4). These torques arise from both inertial and aerodynamic effects, and the difference $\tau^L - \tau^R$ comprises the net roll torque experienced by the FWMAV airframe during flight. These torques are also transmitted through the kinematic structure, appearing on the balance beam after magnification by the transmission ratios $\frac{\partial \phi^L}{\partial q_2}$ and $\frac{\partial \phi^R}{\partial q_2}$ for the torques from the left and right wings, respectively.

In a completely symmetric system, these torques cancel exactly and the balance beam undergoes no rotation. However, should an asymmetry arise, a net torque will appear on the balance beam, causing it to rotate. This rotation alters the stroke velocities of each wing; if the torque from a wing is too low its stroke velocity increases in comparison to the stroke velocity of the opposing wing. This passive modulation of wing stroke trajectories tends towards cancellation of any asymmetric roll torques experienced by the airframe. Further details on this passive dynamic mechanism are given in Sreetharan and Wood (2010).

5 Theoretical simulation

5.1 Actuation

Actuator drive voltage is the single input to the simulation model. Using results from a laminate plate theory analysis, the first bending mode of the cantilever power actuator has been modeled as a grounded spring in parallel with a voltage-proportional force (Wood et al. 2005). The cantilever beam has a linear spring constant of 467 mN/mm, and under a 100 V amplitude sinusoidal drive signal, the actuator exerts a 120 mN amplitude sinusoidal force. The drive signal is applied at 110 Hz, near mechanical resonance to increase stroke amplitude and limit reactive power.

5.2 Mechanical model

The transmission mechanism along with the wing hinge has been treated using a pseudo rigid body model (Howell 2001). All carbon fiber links are assumed to be infinitely stiff, while polymer flexure interconnects have been modeled as perfect revolute joints in parallel with linear torsion springs. Spring constants for the transmission joints and

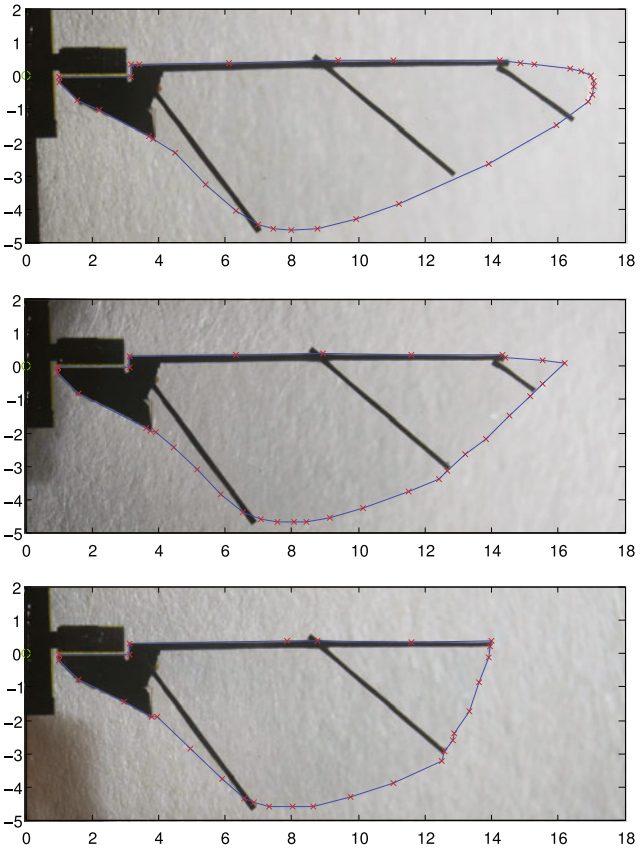

Fig. 5 The wing with membrane outline indicated for the Uncut, 1-Cut, and 2-Cut trials, *from top to bottom*. Axis units are in mm. To properly orient inertial components from Table 1, the z and x coordinate axes correspond to horizontal and vertical image axes, respectively

wing hinges have been calculated using classical beam theory, and no damping or other internal loss mechanisms have been modeled.

The wings themselves are the only significant inertias within the system and are the only inertias considered in the model. The mass of the SCM linkage mechanism is neglected. Though the piezoelectric actuator mass is significant, due to the large transmission ratio the effective inertia of the actuator is negligible and has been omitted from the model.

The final theoretical system has four degrees of freedom: two are contained within the Drag PARITy transmission, while the two wings each add a degree of freedom from their respective wing hinges. The orientation of each wing can be fully described by the angle of the corresponding transmission output (the 'stroke angle' ϕ) and the deflection angle of the wing hinge (the 'rotation angle' ψ), illustrated for the right wing in Fig. 3c.

5.3 Aerodynamic model

Aerodynamic effects have been simulated using a model derived from the blade element method, assuming a perfectly rigid wing planform. As modeled, lift and drag torques are proportional to $\dot{\phi}^2$, the square of stroke velocity. Averaged lift and drag coefficients, strong functions of the rotation angle ψ, were taken from experimental data collected from dynamically scaled models of a fruit fly wing flapping in mineral oil (Dickinson et al. 1999). Calculation of wing rotational moments, important for realizing passive wing rotation, relies on additional experimental work quantifying a non-dimensional center of pressure location $\hat{d}_{cp}$ of fruit fly wings (Dickson et al. 2006; Whitney and Wood 2010). Rotational damping, proportional to $\dot{\psi}^2$, the square of wing rotational velocity, has been modeled in accordance with experimental and theoretical work on tumbling plates (Andersen et al. 2005).

Table 1 Inertial and aerodynamic parameters used for the left and right wings for the Uncut, 1-Cut, and 2-Cut trials. All values have units of mg mm^2. The coordinate frame for inertial components is described in Fig. 5

Wing trial	Left *All*	Right *Uncut*	Right *1-Cut*	Right *2-Cut*
I_{xx}	49.0	47.1	40.6	32.8
I_{yy}	50.5	48.6	42.0	34.1
I_{zz}	1.56	1.49	1.43	1.29
I_{xz}	4.20	3.87	3.38	2.97
Ω_1	46.8	38.2	28.7	21.2
Ω_2	0.587	0.438	0.419	0.387
Ω_3	17.5	13.5	10.6	9.10
Ω_4	0.712	0.952	0.787	0.691

The complete aerodynamic model can be distilled into the following four aerodynamic moments applied to each wing:

$$M_N = -\Omega_1 \mathrm{sgn}(\dot{\phi})\dot{\phi}^2 C_N(\psi) \tag{1}$$

$$M_T = -\Omega_1 \mathrm{sgn}(\dot{\phi})\dot{\phi}^2 C_T(\psi) \tag{2}$$

$$M_{rd} = -\Omega_2 \mathrm{sgn}(\dot{\psi})\dot{\psi}^2 C_{rd} \tag{3}$$

$$M_r = -\left(\Omega_3 \hat{d}_{cp}(\psi) - \Omega_4\right) \mathrm{sgn}(\dot{\phi})\dot{\phi}^2 C_N(\psi) \tag{4}$$

In the previous set of equations, M_T acts about an axis perpendicular to the wing plane and is the result of aerodynamic forces acting in the wing plane. M_r and M_{rd} are the rotational and rotational damping moments, respectively, both acting on the wing around the wing hinge axis. M_N acts about an axis perpendicular to both the wing plane normal and the hinge axis, and results from aerodynamic forces normal to the wing. The three aerodynamic coefficients, related to tangential (C_T), normal (C_N), and rotational damping (C_{rd}) aerodynamic forces, are described in Whitney and Wood (2010). These four aerodynamic moments are treated in the dynamic model as generalized torques.

The parameters Ω_1, Ω_2, Ω_3, and Ω_4 have units of mg mm^2 and can be calculated from the air density ρ and the specific wing morphology (see Table 1 for calculated values). Related work has produced extensive experimental data verifying that this aerodynamic model adequately describes passive rotation of a single wing executing a predetermined stroke angle trajectory, along with generated lift forces (Whitney and Wood 2010). This referenced work contains a detailed description of the aerodynamic model briefly summarized here.

5.4 Mathematical formulation

For the theoretical model, the four coordinates specifying the device configuration were taken to be the left and right wing stroke angles (ϕ^L and ϕ^R, respectively) along with the left and right wing rotation angles (ψ^L and ψ^R, respectively). These four quantities and their time derivatives $\dot{\phi}^L$, $\dot{\phi}^R$, $\dot{\psi}^L$, and $\dot{\psi}^R$ form the full eight element state vector of the dynamic system.

The body inertia of a robotic 100 mg FWMAV is assumed to be orders of magnitude larger than the wing inertias. This assumption is representative of many biological insects, though some exceptions exist (e.g. butterflies). Accordingly, the body frame has been treated as an inertial reference frame for the purpose of predicting wing dynamics. This assumption accurately represents the grounded-airframe experiment undertaken in Sect. 7. Furthermore, theoretical wing dynamic predictions are not expected to be impacted significantly by the non-inertial nature of the body frame of a free flying FWMAV.

The equations of motion for the wings were derived from an Euler-Lagrange formulation assuming a fixed body frame. Since the only modeled inertias in the system are those of the two wings, the form of kinetic energy T is straightforward:

$$T = \frac{1}{2}\left(\boldsymbol{\omega}^L\right)^T \boldsymbol{I}^L \boldsymbol{\omega}^L + \frac{1}{2}\left(\boldsymbol{\omega}^R\right)^T \boldsymbol{I}^R \boldsymbol{\omega}^R \tag{5}$$

In the preceding equation, $\boldsymbol{I}^L$ and $\boldsymbol{I}^R$ are the inertial tensors of each wing, constant in the wing frame and calculated about an origin defined by the closest point on the wing hinge axis to the shoulder axis (see Table 1 for calculated values). The small shoulder offset of the Drag PARITy transmission has been neglected, thus no translational kinetic energy terms are present. The term $\boldsymbol{\omega}^L$ is the angular velocity of the left wing, a function of ϕ^L, ψ^L, $\dot{\phi}^L$, and $\dot{\psi}^L$. An analogous statement applies to the right wing angular velocity $\boldsymbol{\omega}^R$.

The potential energy V has the following form:

$$V = \frac{1}{2}\sum_{i=1}^{9} k_i \gamma_i^2 + \frac{1}{2} k_a q_1^2 \tag{6}$$

The full device contains nine polymer flexure joints: two wing hinges along with seven internal to the Drag PARITy transmission. The quantities γ_i represent the angular deflection of each flexure joint, functions of ϕ^L, ψ^L, ϕ^R, and ψ^R. The constants k_i represent the linearized torsional spring constants for each polymer flexure joint. The constant k_a is a linear spring constant describing the restoring force of the actuator in response to its linear deflection q_1, itself a function of ϕ^L and ϕ^R.

The Lagrangian L is defined as $L = T - V$, and the equations of motion are derived from the Euler-Lagrange equations for each of the $p_i \in \{\phi^L, \psi^L, \phi^R, \psi^R\}$:

$$\frac{\mathrm{d}}{\mathrm{d}t}\frac{\partial L}{\partial \dot{p}_i} - \frac{\partial L}{\partial p_i} = \tau_i \tag{7}$$

Actuation force as well as aerodynamic torques appear in the model as generalized forces τ_i. Actuation occurs along q_1 (see Fig. 3) and aerodynamic torques are more naturally calculated in the wing frame, so the appropriate Jacobians have been used to map these forces onto the configuration variables.

All necessary Jacobian matrices and partial derivatives have been derived in closed analytical form for use within the model, but the details have been omitted for brevity. The four 2nd order differential equations produced from (7) were expressed as a first order system of eight coupled nonlinear differential equations. All theoretical results for the Drag PARITy design are the result of numerically integrating these differential equations using a Runge-Kutta based method as implemented by the MATLAB function ode45.

The theoretical dynamics model has been used to investigate the reaction torque regulating properties of the system in response to wing asymmetry. The system was compared with a baseline design in which the Drag PARITy transmission has been replaced with a conventional transmission characterized by fully actuated wing stroke angles. This baseline design is realized by freezing the degree of freedom q_2 of the Drag PARITy to $q_2 = 0$ (equivalent to the constraint $\phi^L = \phi^R$). This constraint is accommodated by introducing a time-dependent Lagrange multiplier to the Lagrangian:

$$L = T - V + \lambda(t) \cdot (\phi^L - \phi^R) \tag{8}$$

In the modified equations of motion given by (7), $\lambda(t)$ is calculated algebraically at each timestep to satisfy the kinematic constraint. It is to be noted that this baseline three degree of freedom design is identical to that of the HMF (Wood 2008).

A control trial, which will be called the 'Uncut' trial, was simulated using a structure mechanically and aerodynamically symmetric to the tolerances achievable with the SCM

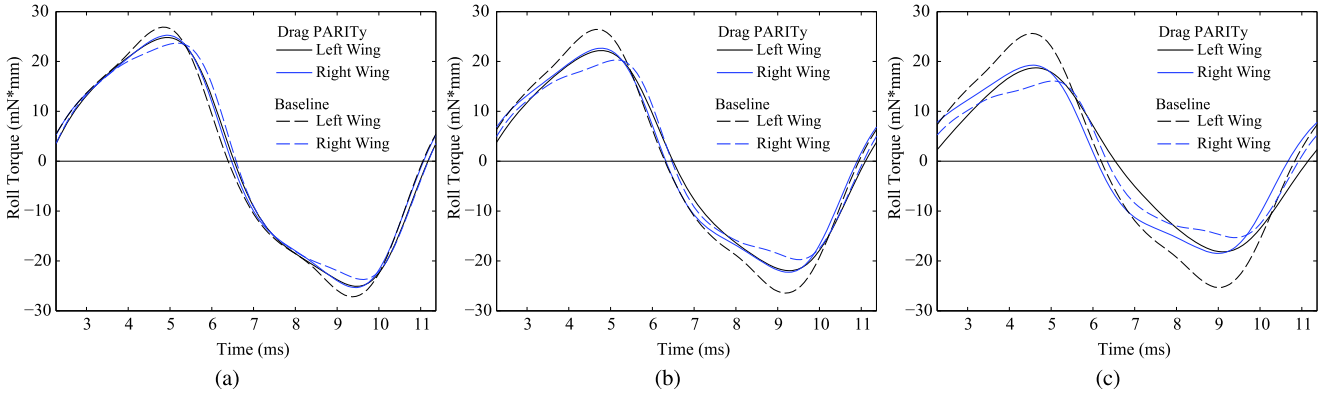

Fig. 6 Theoretical roll torque imparted to the airframe by each wing in the (**a**) Uncut, (**b**) 1-Cut, and (**c**) 2-Cut trials. The difference between the roll torques imparted by the left and right wings appears as a net body torque on the airframe

manufacturing process. Two additional trials were undertaken with intentionally asymmetric wing parameters, realized by removing successive amounts of planform area from the distal extent of the right wing. These trials will be called the 1-Cut and 2-Cut trials, respectively. Images of the right wing planform for all three trials are shown in Fig. 5. The left wing is nominally identical to the Uncut right wing for all three trials.

The wing parameters for the 'Uncut' trial were chosen to imitate those proven to enable tethered take-off in Wood (2008). Since neither wing fabrication, mounting, nor the removal of wing area were precision processes, all wing parameters were measured directly from wings in situ on the experimental test structure. Inertia tensors for the wing were constructed using a baseline mass measurement coupled with a photogrammetric process to determine the spatial distribution of wing mass. Aerodynamic parameters for the wings were calculated using the photogrammetrically determined wing planform areas shown in Fig. 5. Fabrication variation has resulted in measurable asymmetry even in the Uncut case, apparent in theoretical and experimental results. See Table 1 for all calculated inertial and aerodynamic parameters.

In all trials, the Drag PARITy design is observed to execute stable wing trajectories qualitatively similar to those executed by biological insects. Wing stroke angles ϕ^L and ϕ^R oscillate over approximately 100° with a rotation angles ψ^L and ψ^R oscillating between ±60°, approximately 90° out of phase. These rotation angles correspond to an angle of attack $\alpha = 90°$ at stroke extents and $\alpha = 30°$ midstroke. Significant yaw torques, illustrated in Fig. 7, result largely from aerodynamic lift, advancing previous work by demonstrating Drag PARITy operation on a lift-generating platform. Theoretical wing trajectories are plotted in Figs. 10a and 10c.

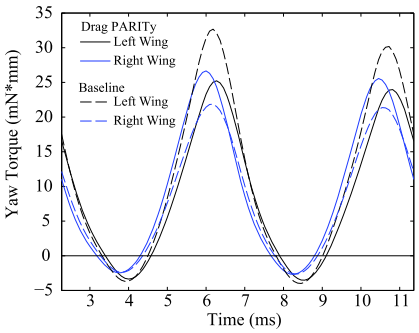

Fig. 7 Yaw torque in the 1-Cut trial

6 Passive body torque regulation

The Drag PARITy design distinguishes itself from the baseline design in the theoretical reaction torques imparted by the flapping wings on the airframe, that is, the quantities τ^L and τ^R mentioned previously. The Drag PARITy is designed to balance the roll reaction torques imparted by the flapping wings. Figure 6 plots the theoretical roll torques experienced by the body of a FWMAV using a Drag PARITy transmission compared to that experienced by a FWMAV using a conventional baseline transmission described previously. Note that these torques are nominally opposing and that it is their difference, $\tau^L - \tau^R$, that is experienced by the body as a net roll torque. In all three trials, it is apparent that the Drag PARITy transmission has succeeded in balancing the roll torques experienced by the body due to each wing. The results are especially striking in the Uncut trial (Fig. 6a), where the transmission has passively compensated for fabrication and assembly error present in the nominally symmetric structure.

In the 2-Cut trial, the Drag PARITy can be seen to produce a visible roll torque imbalance. The cause of this imbalance is the existence of a small spring torque within the

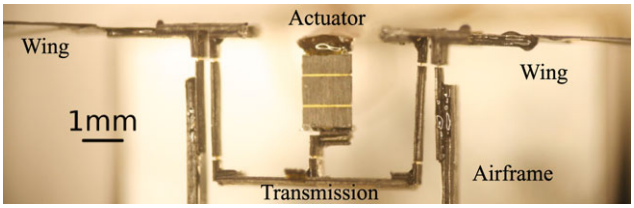

Fig. 8 Front view of the experimental device

transmission which opposes differences in wing stroke angles $\phi^L - \phi^R$. In normal operation, this torque prevents slow drift of the wing stroke midpoint. However, the stroke amplitude difference in the 2-Cut trial is large enough such that this spring torque appears as a net roll torque imbalance on the airframe. The magnitude of this spring torque is an important design consideration, and further details are given in Sreetharan and Wood (2010).

Another interesting result of this theoretical study is the indirect balancing of yaw torques. Yaw torques, referring to Fig. 2, result from aerodynamic lift generated by the wings along with inertial coupling due to wing rotation; no yaw torques were generated in previous work incorporating fixed wing rotation (Sreetharan and Wood 2010). The results for the 1-Cut trial are presented in Fig. 7. In the drastically asymmetric 1-Cut and 2-Cut trials, use of the Drag PARITy design reduces the large average yaw torque imbalance imparted on the airframe by 71% and 72% respectively. However, in the nominally symmetric Uncut case, the Drag PARITy did not reduce the small average yaw error torque.

7 Experimental verification

After acquiring data for the Uncut trial, the right wing was cut in situ to conduct the 1-Cut and 2-Cut trials without perturbing the alignment of the wing on the transmission output. As previously mentioned, all dynamic wing parameters were measured without disturbing the device and are presented in Table 1.

Two high speed video cameras were positioned such that each obtained a clear view of both wings over the entire flapping motion. Prior to acquiring video, the cameras were calibrated using routines from the CalTech Camera Calibration Toolbox for MATLAB (Bouguet 2008). Once calibrated, the toolbox allows reconstruction of three dimensional coordinates of points identified in both camera views.

A 110 Hz 200 V (peak to peak) sinusoidal voltage was applied to the power actuator and synchronized high speed video was acquired from both video cameras at 10,000 fps, or 91 frames per wingstroke period. Sample still frames are shown in Fig. 9.

Three easily distinguished features of the wing venation pattern were manually tracked across 300 frames for each

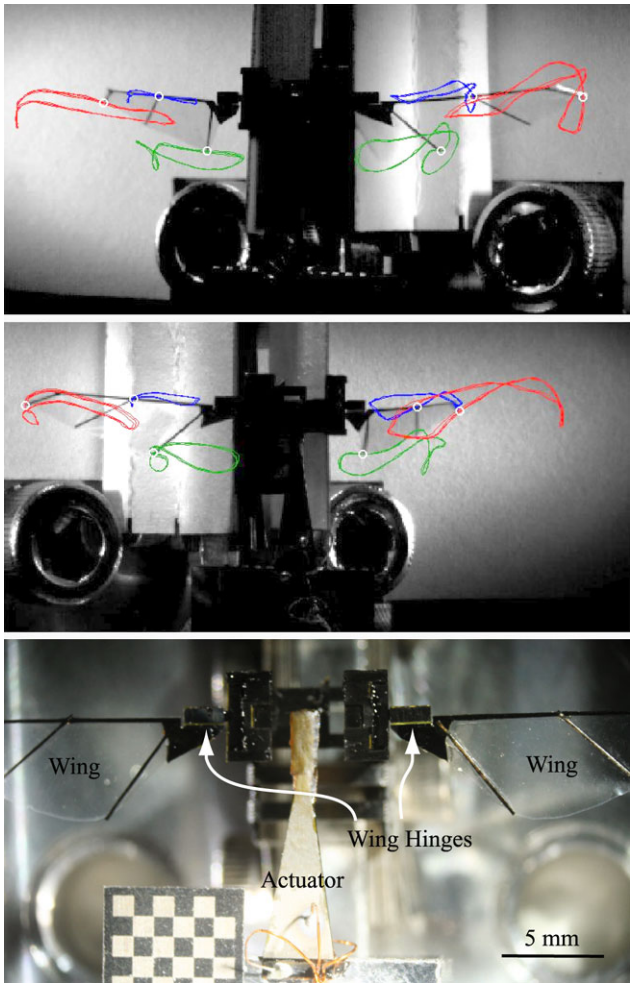

Fig. 9 *Upper images* are synchronized frames from the two cameras during the Uncut trial. *Tracked points* are indicated along with their trajectories over the course of the video. *Lower image* illustrates test structure

trial. Identification of all three points in two camera views allows stereophotogrammetric reconstruction of the full wing orientation. The sinusoidal drive voltage applied to the actuator has been recorded and digitized at 5 kHz, synchronized with the high speed video stream.

The observed stroke and rotation angles are plotted as a function of time in Fig. 10, along with predictions produced by the theoretical model. Time synchronization has been achieved by aligning the theoretical and experimental drive signals, omitted from the plots for clarity. The functional form of the applied voltage signal as a function of time (in seconds) is:

$$V(t) = 100V + 100V \cdot \sin(110 \cdot 2\pi t) \tag{9}$$

From Fig. 10, it is immediately apparent that the theoretical model accurately captures qualitative characteristics of the experimental model, with rotation angle ψ exhibiting an approximately 90° phase lag behind the stroke angle ϕ. Fur-

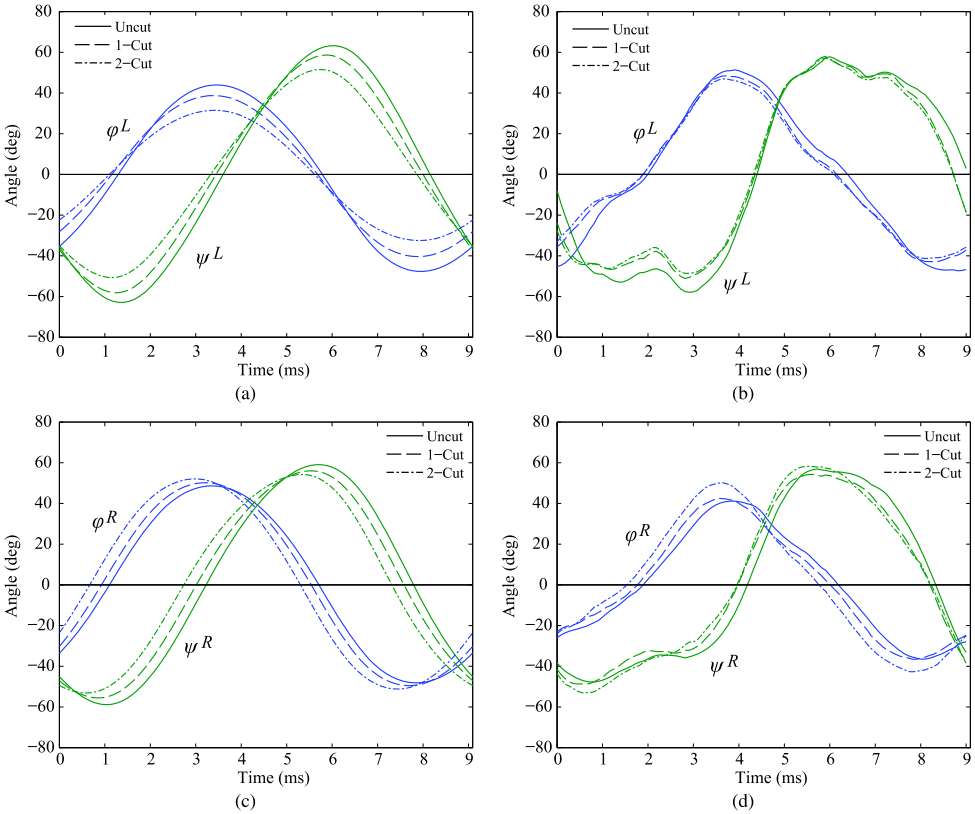

Fig. 10 Left wing trajectories (**a**) predicted by theory and (**b**) observed experimentally, along with (**c**) theoretical and (**d**) experimental right wing trajectories. Wing stroke angle trajectories ϕ^L and ϕ^R adapt to compensate for asymmetric wing parameters; rotation angles ψ^L and ψ^R are also impacted

thermore, the theory also accurately predicts oscillation amplitudes from applied drive voltage, no small achievement considering the complexity of this nonlinear dynamic system.

Theoretically predicted trends in wing trajectories as the right wing planform is altered are apparent in experimental data. The model predicts a monotonic increase in $\phi^R(t)$ amplitude as planform area is successively removed from the right wing, coupled with an associated decrease in the amplitude of $\phi^L(t)$. This trend is reflected in the experimental data as the Drag PARITy transmission passively diverts additional power to the underperforming right wing. The model also predicts a successive decrease in the amplitudes of both wing rotations $\psi^L(t)$ and $\psi^R(t)$ as wing membrane is removed. This trend is apparent in the observed trajectory of $\psi^L(t)$, though somewhat ambiguous in the observed trajectory of $\psi^R(t)$.

Among features not predicted by this simulation model are the square-wave appearance of observed wing rotations and the complex non-sinusoidal details of stroke angle trajectories. In future work, it is hoped that these discrepancies will be reduced by a more detailed theoretical model including, for example, mechanical loss mechanisms and nonlinear descriptions of polymer flexures to better predict dynamic characteristics at large joint angles. The transmission design itself will be refined to limit unintended and difficult to model behavior. For example, one source of error in this experimental trial was off-axis transmission compliance, resulting in measurable deviation of the wings from their mean stroke planes.

8 Conclusion and future work

This paper has presented further evidence supporting the utility of passive underactuated mechanisms in FWMAVs. Significantly extending previous work, the load balancing Drag PARITy transmission has been shown to be compatible with longitudinally compliant wing hinges allowing passive variation of wing angle of attack. The resulting singly actuated four degree of freedom system has been shown to execute stable qualitatively biomimetic flapping wing trajectories well described by the associated theoretical model. Furthermore, the Drag PARITy transmission is shown to maintain its load balancing capabilities, passively altering wing trajectories so as to balance roll torques experienced by the FWMAV airframe.

Future work exploring the PARITy methodology will proceed along two parallel tracks:

1. Demonstrating long timescale control mechanisms
2. Expanding passive regulation to larger subsets of body forces and torques.

As previously mentioned, long timescale control in PARITy enabled FWMAVs will be achieved not by direct modulation of wing kinematic trajectories, but by active modification of system dynamics. For example, the Drag PARITy transmis-

sion described in this paper exhibits short timescale dynamics that balance roll torques from each wing. An active control input could be introduced to bias these dynamics such that they passively regulate the ratio of roll torques τ^L and τ^R from the left and right wings, respectively, to a specified setpoint q_3:

$$\tau^L/\tau^R = q_3 \tag{10}$$

Note that q_3 is fixed at unity for the simple Drag PARITy transmission. A variety of dynamic parameters within the transmission, such as spring constants and link lengths, can be actively modulated at long timescales to realize this biased short timescale behavior. The potential for simple control relationships such as (10), bypassing wing kinematics to directly concern airframe forces and torques, is an exciting result of the PARITy methodology. Demonstration of such control features will motivate one track of future work.

A second research track involves introducing alternative or additional passive degrees of freedom to an FWMAV drivetrain to regulate different or expanded subsets of the body forces and torques produced by the wings. The Drag PARITy drivetrain is a mechanically intelligent device that has demonstrated regulation of body roll torques, arising in part from aerodynamic drag. In one nascent concept, careful introduction of passive features may enable an FWMAV drivetrain that directly regulates yaw torques arising from aerodynamic lift in addition to roll torques. The design space of such mechanically intelligent structures is vast, and future work will attempt to produce a variety of force and torque regulating FWMAV structures.

The PARITy methodology has the potential to simplify flight control of insect-scale robotic FWMAVs. It is hoped that future research into this novel methodology will provide tools to increase aerodynamic performance and reduce requisite system complexity, hastening the arrival of an autonomous 100 mg-scale robotic FWMAV.

Acknowledgements The authors gratefully acknowledge support from the National Science Foundation (Award No. CMMI-07466 38). Any opinions, findings and conclusions or recommendations expressed in this material are those of the authors and do not necessarily reflect those of the National Science Foundation.

References

Andersen, A., Pesavento, U., & Wang, Z. (2005). Unsteady aerodynamics of fluttering and tumbling plates. *Journal of Fluid Mechanics*, *541*, 65–90.

Bouguet, J. Y. (2008). Camera calibration toolbox for matlab. http://www.vision.caltech.edu/bouguetj/calib_doc/index.html.

Deng, X., Schenato, L., & Sastry, S. (2006). Flapping flight for biomimetic robotic insects: Part ii—flight control design. *IEEE Transactions on Robotics*, *22*(4), 789–803.

Dickinson, M. H., Lehmann, F. O., & Sane, S. P. (1999). Wing rotation and the aerodynamic basis of insect flight. *Science*, *284*, 1954–1960.

Dickson, W. B., Straw, A. D., Poelma, C., & Dickinson, M. H. (2006). An integrative model of insect flight control. In *Proceedings of the AIAA aerospace sciences meeting and exhibit*, Reno, NV.

Fearing, R. S., Chiang, K. H., Dickinson, M. H., Pick, D. L., Sitti, M., & Yan, J. (2001). Wing transmission for a micromechanical flying insect. *Journal of Micromechatronics*, *1*(3), 221–237.

Howell, L. L. (2001). *Compliant mechanisms*. New York: Wiley.

Sreetharan, P. S., & Wood, R. J. (2010). Passive aerodynamic drag balancing in a flapping wing robotic insect. *Journal of Mechanical Design*, *132*(5), 051006. doi:10.1115/1.4001379.

Whitney, J. P., & Wood, R. J. (2010). Aeromechanics of passive rotation in flapping flight. *Journal of Fluid Mechanics*, *660*, 197–220. doi:10.1017/S002211201000265X.

Wood, R. J. (2008). The first takeoff of a biologically inspired at-scale robotic insect. *IEEE Transactions on Robotics*, *24*, 341–347.

Wood, R. J., Steltz, E., & Fearing, R. S. (2005). Optimal energy density piezoelectric bending actuators. *Sensors and Actuators. A, Physical*, *119*(2), 476–488.

Wood, R. J., Avadhanula, S., Sahai, R., Steltz, E., & Fearing, R. S. (2008). Microrobot design using fiber reinforced composites. *Journal of Mechanical Design*, *130*(5), 052304. doi:10.1115/1.2885509.

P.S. Sreetharan holds a bachelor's degree in Physics from Harvard University (2006), where he conducted research with Harvard's optical search for extraterrestrial intelligence (Optical SETI). As a research physicist at ThermoFisher Scientific, he has earned several patents on hand-held analysis instruments based on both x-ray fluorescence and optical emission spectroscopic techniques. He is now a Ph.D. candidate at Harvard University, where his research interests include flapping wing flight, dynamic modeling, and underactuated robotic systems. Extending his research interests, he enjoys highly dynamic activities including running, bicycling, skiing, and flying.

R.J. Wood is an Associate Professor in Harvard's School of Engineering and Applied Sciences and core faculty member of the Wyss Institute for Biologically Inspired Engineering. Prof. Wood completed his M.S. (2001) and Ph.D. (2004) degrees in the Dept. of Electrical Engineering and Computer Sciences at the University of California, Berkeley. He is founder of the Harvard Microrobotics Lab where his research interests include the creation of biologically-inspired aerial and ambulatory microrobots, the unsteady aerodynamics of flapping-wing flight, minimal control of under-actuated computation-limited systems, decentralized control of multi-agent systems, artificial muscles, and morphable soft-bodied robots. He is the winner of a 2007 DARPA Young Faculty Award, a 2008 NSF Career Award, a 2008 ONR Young Investigator Award, a 2008 Air Force Young Investigator Award, multiple best paper and best video awards, and is a member of the 2008 class of Technology Review's TR35. In January 2010 he received a Presidential Early Career Award for Scientists and Engineers from President Obama.